Venous Collagenosis as Pathogenesis of White Matter Hyperintensity

David Lahna, BA ,[1] Daniel L Schwartz, BA,[1,2] Randy Woltjer, MD, PhD,[3]

Sandra E Black, MD,[4,5,6] Natalie Roese, MPH,[1] Hiroko Dodge, PhD,[1] Erin L Boespflug, PhD,[1]

Julia Keith, MD,[7] Fuqiang Gao, MD,[4,5] Joel Ramirez, PhD ,[4,5] and Lisa C Silbert, MD[1]

Objective: Periventricular white matter hyperintensities (pvWMHs) are commonly observed on MRI in older individuals and are associated with cognitive and motor decline. The etiology of pvWMH remains unknown. Venous collagenosis has been implicated, which may also interfere with perivascular fluid flow leading to dilation of perivascular spaces (PVS). Here, we examine relationships between in vivo pvWMH volume and ex vivo morphological quantification of collagenosis and the PVS in veins and arteries.

Methods: Brain tissue from 25 Oregon Alzheimer's Disease Research Center subjects was selected to cover the full range of WMH burden. Tissue from white matter abutting the ventricle was stained with Masson's trichrome and smooth muscle actin. An automated hue based algorithm identified and segmented vessel into collagenized vessel walls, lumen, and PVS. Multiple linear regressions with pvWMH volume as the dependent variable and either collagen thickness or PVS width were performed with covariates of vessel diameter, age at death, sex, and interval between MRI and death.

Results: PVS width and collagen thickness were significantly correlated in both arteries ($r = 0.21$, $p = 0.001$) and veins ($r = 0.23$, $p = 0.001$). Increased venous collagen ($p = 0.017$) was a significant predictor of higher pvWMH burden while arterial collagen was not ($p = 0.128$). Neither PVS width in arteries ($p = 0.937$) nor veins ($p = 0.133$) predicted pvWMH burden.

Interpretation: These findings are consistent with a model in which venous collagenosis mediates the relationship between vascular risk factors and pvWMH. This study confirms the importance of changes to the venous system in contributing to MRI white matter lesions commonly observed with advanced age.

ANN NEUROL 2022;92:992–1000

Introduction

White matter hyperintensities (WMHs), prominently visible as regions of high signal intensity within parenchymal tissue relative to normal appearing white matter on T_2/FLAIR-weighted MRI, are a common finding in the aged population. A positive relationship exists between WMH volume and the risk of stroke, mild cognitive impairment, dementia, and overall mortality,[1–4] although the mechanistic

details of these relationships remain elusive. These lesions can be divided by their location into periventricular and deep[5]; diffuse periventricular WMH (pvWMH) are more often observed at the frontal and posterior horns of the lateral ventricle and extend superolaterally, while deep WMH are often punctate lesions that appear in the centrum semiovale in subcortical white matter (WM).

Many post mortem studies have demonstrated a significant relationship between MRI visible WMH and arteriolosclerosis.[6–10] Although veins are rarely examined, some previous studies have identified thickening of cerebrovascular walls in WM associated with or proximal to WMH and concluded that the venous system is particularly implicated.[7,11,12] Surgical and genetic animal models used to induce hypertension have reliably demonstrated causal relationships between hypertension and cerebrovascular venous wall sclerosis and thickening due to collagenosis[13]; some have further observed WMH-like periventricular lesions,[14] leading them to conclude that venous collagenosis may cause ischemic WM damage.

A recent *in vivo* MRI study with *post mortem* histopathology in humans[15] confirmed the relationship described by Moody et al.[11] between venous collagenosis and pvWMH. Investigators hypothesized that venous collagenosis increased the rigidity of veins, thereby disrupting perivenular fluid flow[15] and leading to stasis of interstitial fluid at or near WMH. Given past and recent work describing fluid transport in the parenchyma alongside vessels in the peri/paravascular space[16,17] and the possibility that pathological fluid stasis in the efflux portion of this system may cause the retrograde buildup of interstitial fluid in the parenchyma, a detailed examination of the effect of small vessel disease in brain parenchyma with respect to pvWMH obliges a morphological quantification of the perivascular spaces (PVS) in periventricular vessels.

This report details the relationships between *in vivo* volume measurements of pvWMH and *ex vivo* morphological quantitation of collagenosis and PVS in periventricular vessels in the same individuals, with a particular focus on vessel lineage. We hypothesize that the degree of venous but not arterial collagenosis is positively associated with pvWMH burden, the size of the PVS in venules is positively correlated with pvWMH burden, and that collagenosis is associated with a proportionally larger PVS in all vessels.

Methods

Data Collection

Brain tissue was obtained from participants previously followed in the NIH-Layton Oregon Alzheimer's Disease Research Center (OADRC) longitudinal aging study with signed autopsy consent. In brief, OADRC participants were community dwelling individuals age 55 years or greater, who underwent detailed cognitive, neurological and MRI assessments. All subjects signed written informed consent and approval from the Institutional Review Board of Oregon Health & Science University was obtained (IRB00000361). Ninety seven deceased OADRC participants who had undergone brain autopsy and who had *in vivo* 1.5 T MRI results were available. MRI were segmented into deep WMH, periventricular WMH, and total intracranial volume using previously described methods.[18] In brief, unambiguous pixels of WMH (as well as brain tissue and fluid) were selected on a dual echo spin echo sequence. A regression model that included proton density and T2 intensities and location of each pixel differentiated tissue types. WMH was identified based on higher signal intensity observed on proton density and T2-weighted contrasts. Areas of high signal that abutted ventricles were defined as being periventricular WMH, whereas areas of high signal that were surrounded by healthy brain tissue were defined as being deep WMH. Available samples were rank ordered by total WMH burden and every fourth dataset was analyzed resulting in 25 samples covering the available range of WMH volumes. The vast majority of samples were from subjects with pure or mixed Alzheimer's diagnoses (n = 23, 92%). The MRI to death interval ranged from 2.6 to 14.3 years with a mean of 6.9 years. Further demographic and diagnostic information can be found in Table 1 including Braak staging, degree of cerebral amyloid angiopathy[19] and presence of infarcts.[20]

Tissue Processing

Brains were examined grossly and microscopically after fixation in neutral-buffered formaldehyde solution for at least 2 weeks, and samples from all cortical lobes, anterior cingulate gyrus, hippocampus, amygdala, striatum, thalamus, midbrain, pons, medulla, and cerebellum were evaluated microscopically using hematoxalin-eosin and luxol fast blue and immunohistochemical studies of tau, beta-amyloid, alpha-synuclein, TDP-43, and ubiquitin to determine diagnostic features as described previously.[6] Similar to Keith et al,[15] three paraffin embedded 6 μm thick coronal blocks of tissue per subject from anterior, middle and posterior superolateral periventricular WM were stained with Masson's trichrome histochemical stain (kit from Newcomer Supply, Middleton, WI) and by immunohistochemistry for the presence of smooth muscle actin (SMA, antibody from Dako USA, Carpinteria, CA), an arterial marker that is relatively diminished in venules. Slides were scanned at a resolution of 0.773 μm^2/pixel and downsampled to 13.4 μm^2/pixel.

Digital Microscopy Segmentation and Analysis

An automated hue based algorithm identified vessels in trichrome images. Decorrelation stretching was applied to the red-green-blue (RGB) images, which were then transformed to hue-saturation-value images (HSV). "Blue" objects (collagen in vessel walls) were detected by finding

TABLE 1. Demographics, Diagnoses, and MRI Variables (N = 25)	
	Mean (SD) Range
Age at death (years)	81.9 (11.75) 54.6 - 99.5
Sex (N, % female)	9 (36%)
MRI-to-death interval (years)	6.9 (2.89) 2.6 – 14.3
Total WMH volume (cc)	7.81 (8.0) 0.22–32.42
pvWMH volume (cc)	6.62 (5.97) 0.02–24.43
Deep WMH volume (cc)	1.19 (2.31) 0–8.48
History of HTN (N, %)	10 (40%)
History of stroke (N, %)	5 (20%)
History of TIA (N, %)	3 (12%)
Pathological diagnosis (N, %)	14 (56%) AD
	3 (12%) minimal AD pathology
	5 (20%) mixed AD/VD
	2 (8%) VD
	1 (4%) mixed AD/LBD
Cerebral amyloid angiopathy (N,%)*	7 (28%) none
	7 (28%) mild
	10 (40%) moderate
	1 (4%) severe
Braak staging (N,%)*	1 (4%) none
	1 (4%) stage 1
	2 (8%) stage 2
	2 (8%) stage 4
	3 (12%) stage 5
	16 (64%) stage 6
Microinfarcts present (N,%)*	14 (56%)
Macroinfarcts present (N,%)*	1 (4%)

SD = standard deviation; cc = cubic centimeter; AD = Alzheimer 's disease; VD = vascular dementia; LBD = Lewy body disease.
*Pathological diagnoses made using NACC criteria.

connected components in the HSV whose hue was between 0.45 and 0.70, saturation > 0.9, and larger than 670 μm². The "holes" (lumenal and other) in the resultant collagen mask were filled, and filled vessel objects were further constrained to be larger than 13400 μm²

which equates to a vessel diameter of 130.62 μm. Vessels smaller than this threshold were removed due to the difficulty of clearly delineating the lumen at that scale. Lumenal (and other holes) were separately segmented by subtracting the collagen mask from the labeled vessel mask. PVS segmentation was accomplished by finding all whitespace objects (pixels in which all RGB channels were valued greater than 200 and which formed connected objects larger than 670 μm²), adding whitespace objects into the binary vessel mask, and relabeling all final summed connected objects. All whitespace objects which were found to have an object label that matched a vessel label were assigned to that vessel; any whitespace objects which were not connected to a vessel object were discarded. Finally, all resulting objects (walls, lumen and other connected holes, and PVS) were subjected to a "tissue mask" constraint in an effort to remove meningeal vessels, that is, all connected components on the entire slide image were identified and the largest object was taken to be the tissue mask. The native RGB image was translated to HSV, thresholded on the saturation channel >0.1, and holes filled.

Eight hundred six identified potential vessels across all samples were visually inspected. Ninety-two objects (11.4%) were excluded for being meningeal vessels (Figure 1, bottom left) or objects other than vessels, 99 objects (12.3%) were excluded for having broken, noncontiguous walls which precluded proper segmentation (Figure 1, bottom middle), and 68 objects (8.4%) were excluded from further analysis because they consisted of contiguous clumps of multiple vessels (Figure 1, bottom right). The remaining 547 objects (67.9%) were segmented into arteries and veins on the basis of SMA positivity.

Slide Coregistration and Vessel Segmentation

SMA slides were registered to trichrome using the following procedure: decorrelation stretching was applied, the RGB images were translated to grayscale, and the grayscale output was downsampled by a factor of 5. The resulting images were rigid registered using Matte's Information Metric (50 bins) for multimodal image registration (MATLAB; Natick, MA), and a modified one-plus-one evolutionary optimizer. Optimizer changes included an initial search radius set at 0.003, the minimum size of the search radius was set to 0.00015, the growth factor rate of the search radius was set to 1.01, and the maximum iterations was set at 1000. After a transformation matrix had been generated, translation elements of the transformation matrix were multiplied by five, the scaled transformation matrix was applied to the original SMA RGB image, and the output was saved in its native imported resolution.
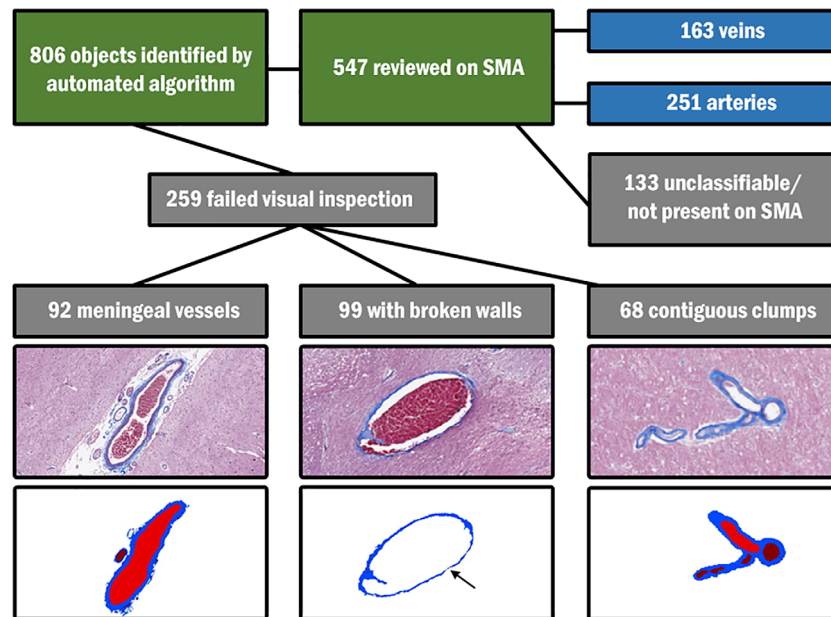
FIGURE 1: Results from automated vessel segmentation algorithm on 75 slides (three slides/subject) stained with Masson's trichrome. Common error classes are shown in three examples along with the automated segmentation result (bottom).

Segmentation results were visually inspected by an experienced neuropathologist (RW) blinded to participant demographics and MRI characteristics. Each vessel was marked as "artery", "vein", or "unclassifiable" as judged by a positive stain on the coregistered SMA slide. One hundred sixty-three of the remaining 547 (28.4%) appropriately segmented vessels were veins, 251 (45.9%) were arteries, and 133 (24.3%) were unclassifiable either because SMA positivity was indeterminate or the vessel could not be identified in the coregistered SMA stain. The final set consisted of 414 vessels (Figure 2).

The average lumen diameter, collagen wall thickness and PVS width for each vessel were calculated by taking the segmentation areas of white space within the vessel (ie, lumen), collagen and extravascular white space and modeling each vessel as a circular lumen surrounded by two concentric annuli, the internal one of collagen and the external PVS (Figure 3).

MRI Analysis

MRI acquisition parameters and segmentation algorithms have been previously described in detail [18,21]. In brief, scans were acquired on a 1.5 T GE system, and a customized, semi-automated image analysis software program, REGION, was used to quantify brain regions of interest. Representative unambiguous voxels of each tissue type including WMH, brain, CSF and bone were selected and then segmented into tissue type using a regression model based on proton density and T_2 signal intensities as well as voxel location. WMH contiguous with the ventricles

was labeled periventricular WMH. ICV was calculated as the sum of brain structures and CSF segmented by REGION. WMH volumes were ICV corrected and log transformed[18] to maintain normal distribution.

Statistical Testing

Pearson correlation coefficients were calculated to assess relationships between PVS width, collagen thickness, vessel lumen diameter, age at death, and distance from the ventricle. T-tests were used to compare distance from the ventricle, vessel diameter, collagen thickness and PVS width between veins and arteries. Multiple linear regressions were used to determine the relationships between WMH and collagen thickness as well as WMH and PVS width while covarying for sex, age at death, MRI-to-death interval, and vessel size (lumen diameter + collagen thickness), using periventricular WMH as the dependent variable.

Results

Differences Between Veins and Arteries

Veins were larger than arteries ($t_{(412)} = -7.87, p < 0.001$) and closer to the ventricles ($t_{(412)} = 10.32, p < 0.001$), but did not differ from arteries in collagen thickness ($t_{(412)} = -1.53, p = 0.127$) or PVS width ($t_{(412)} = -0.66, p = 0.512$). Means and standard deviations of vessel characteristics can be found in Table 2.

PVS Width. PVS width of veins was positively correlated with collagen thickness ($r_{(161)} = 0.23, p = 0.003$) and
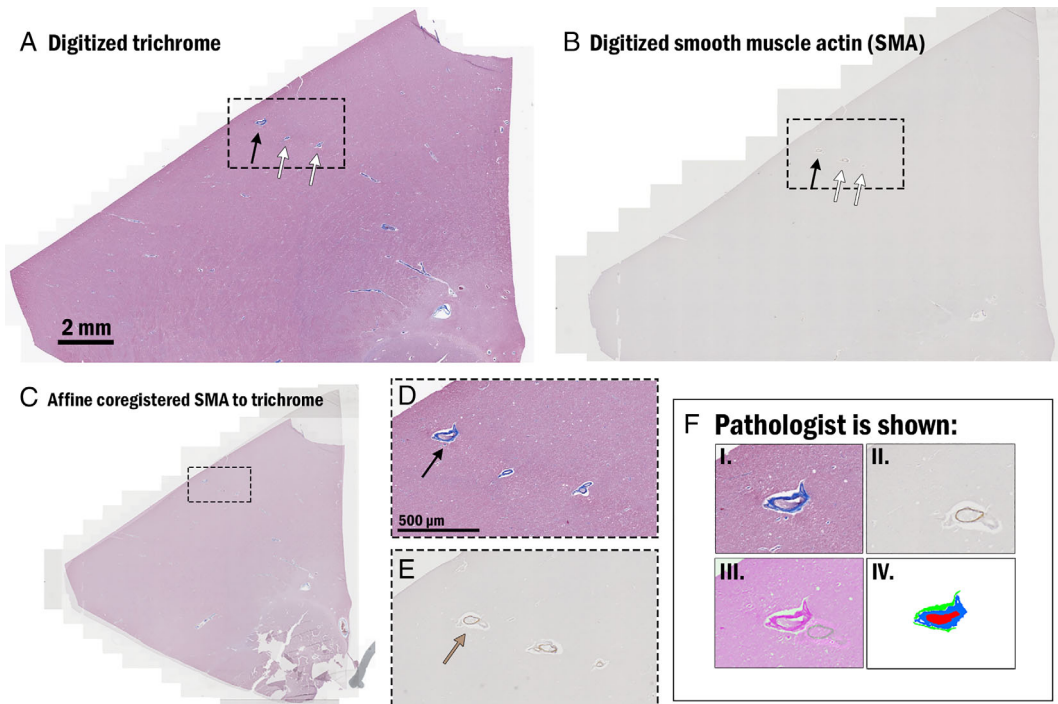
FIGURE 2: Trichrome (A)- and SMA-stained (B) slides from the same cartridge are shown along with the results of the whole-slide affine registration (C), zoomed views of trichrome (D), and SMA (E), and the images the neuropathologist (R.W.) was shown for designating the lineage of the vessel: F(I) is the native trichrome image, F(II) is the native SMA depicting an artery, F(III) represents the whole-slide registration between the two (the trichrome slide has been falsely colored pink and the SMA green for ease of viewing, and finally F(IV) depicts the final segmentation of the vessel (green is PVS, blue is collagen, and red is lumen).

female sex ($r_{(161)} = 0.24$, $p = 0.002$) but not significantly correlated with vein diameter ($r_{(161)} = 0.02$, $p = 0.8$), nor age at death ($r_{(161)} = 0.34$, $p = 0.13$).

PVS width of arteries was positively correlated with collagen thickness ($r_{(249)} = 0.21$, $p < 0.001$) but not significantly correlated with arterial diameter ($r_{(249)} = 0.07$,

$p = 0.29$), nor age at death ($r_{(249)} = 0.14$, $p = 0.49$) or sex ($r_{(249)} = 0.01$, $p = 0.89$).

Collagen Thickness. Venous collagenosis was positively correlated with vessel diameter ($r_{(161)} = 0.54$, $p < 0.001$), age at death ($r_{(161)} = 0.45$, $p = 0.036$) and female sex
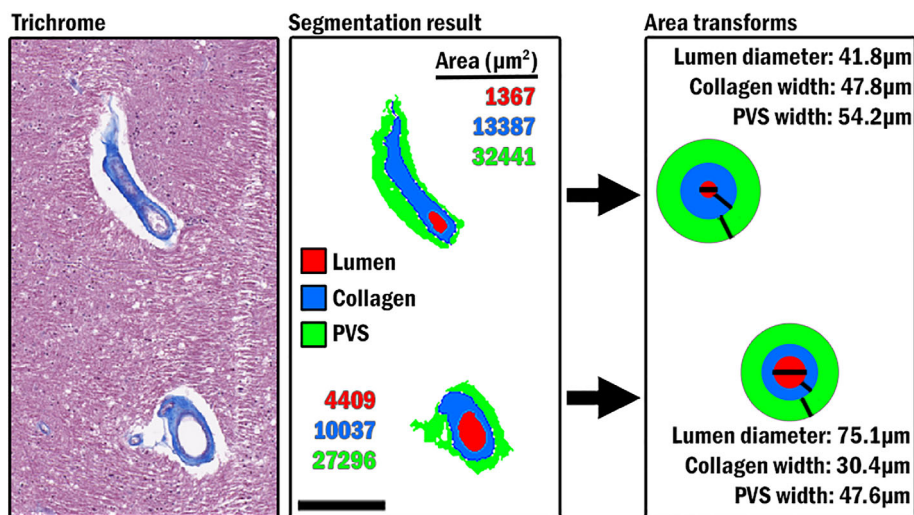
FIGURE 3: Segmentation and quantitation method for two nearby vessels. The area of vessels that passed manual quality assurance and were identifiable as an artery or vein was reorganized into a circle (lumen) and two concentric annuli (collagen, and PVS) while conserving their area (colored quantities, middle). The diameter of the lumen, the width of the wall annulus, and the width of the PVS annulus were taken as the dependent variables that described the vascular unit (right).

TABLE 2. Vessel Characteristics

		Mean (SD)
Vessel diameter (μm)	Arteries	209.4 (86.0)
	Veins	327.0 (212.4)
Distance from ventricles (mm)	Arteries	8.57 (4.66)
	Veins	4.12 (3.64)
Collagen thickness (μm)	Arteries	33.4 (13.8)
	Veins	36.3 (24.9)
PVS width (μm)	Arteries	32.1 (33.1)
	Veins	35.3 (66.1)

($r_{(161)} = 0.17$, $p = 0.032$). Arterial collagenosis was correlated with vessel diameter ($r_{(249)} = 0.51$, $p < 0.001$) but not age at death ($r_{(249)} = 0.29$, $p = 0.17$) or sex ($r_{(249)} = -0.87$, $p = 0.172$).

Relationship Between Venous and Arterial Collagen Thickness and pvWMH Burden. Multiple linear regressions, with %WMH volume as the dependent variable and vessel collagen thickness as the independent variable were performed. The first model included venous collagen thickness and the second model included arterial collagen thickness as independent variables. Covariates in both models included vessel diameter, age at death, sex, and time interval between *in vivo* MRI and death. In model number 1 (venous), a significant overall regression equation was found ($F_{(5,157)} = 34.226$, $p < 0.001$ $R^2 = 0.522$). Female sex ($p = 0.006$), older age at death ($p < 0.001$), shorter interval between MRI and death ($p < 0.001$), smaller vein diameter ($p = 0.007$), and increased venous collagen thickness ($p = 0.017$) were all significant predictors of higher pvWMH burden. In model number 2 (arterial), the overall model was significant ($F_{(5,245)} = 9.802$, $p < 0.001$, $R^2 = 0.167$), but arterial collagen thickness was not a significant predictor of pvWMH burden ($p = 0.128$) nor was arterial vessel diameter ($p = 0.191$). Female sex ($p = 0.002$), older age at death ($p < 0.001$) and shorter interval between MRI and death ($p = 0.007$) remained significant predictors of a higher pvWMH burden. See Table 3 for an overview of these results.

Relationship Between Venous and Arterial PVS Width and pvWMH Burden. Multiple linear regressions, with % WMH volume as the dependent variable and vessel PVS width as the independent variable were performed. The first model included venous PVS width and the second model included arterial PVS width as independent variables. Covariates in both models included vessel diameter, age at death, sex, and time interval between *in vivo* MRI and death. In model number 1 (venous), a significant overall regression equation was found ($F_{(4,158)} = 39.886$, $p < 0.001$, $R^2 = 0.502$). Venous PVS width was not a significant predictor of pvWMH burden ($p = 0.133$). Female sex ($p = 0.013$), older age at death ($p < 0.001$), and shorter interval between MRI and death ($p < 0.001$) were all significant predictors of pvWMH burden. In model number 2 (arterial), the overall model was significant ($F_{(4,246)} = 11.496$, $p < 0.0001$, $R^2 = 0.157$). However, PVS width around arteries was not a significant predictor of pvWMH burden ($p = 0.937$); female sex ($p = 0.001$), older age at death ($p < 0.001$), and shorter interval between MRI and death ($p = 0.003$) remained significant predictors of pvWMH burden. See Table 3 for an overview of these results.

Discussion

This report confirms several previously reported anatomical and histopathological findings: (1) veins are larger than arteries in white matter near the ventricle[22] and (2) that aging and sex are predictive factors for pvWMH burden. Although several studies have found a relationship between WMH burden and venous collagenosis[11,15,23] no previous study has directly compared collagen thickness surrounding veins with that of surrounding arteries in relation to *in vivo* MRI WMH burden. This current study has uniquely demonstrated that collagenosis involving veins but not arteries, in the same tissue samples, is associated with the degree of MRI-visible WMH volume surrounding the ventricle in older individuals. The size of the PVS around a vessel, regardless of the lineage, is correlated with the degree of collagenosis in the vessel wall; although veins are larger than arteries, the walls of vessels identified as veins did not contain more collagen or have a larger PVS than arteries, and the size of the PVS in either veins or arteries was not a predictor of pvWMH burden.

A decrease in parenchymal fluid clearance has been suggested to be associated with pvWMH[24] rather than an increase in fluid deposition as in vasogenic edema. Supported by the evidence presented in this report and in other recent reports[7,15] venous collagenosis may cause parenchymal fluid stasis and potentially mediate the relationship between vascular risk factors and pvWMH. As arteries stiffen as a consequence of aging and associated arteriosclerosis, they are less able to dampen and absorb the increased range of cardiac output pressure. Increased

TABLE 3. Predictors of pvWMH Burden

Model	Significance	Covariates			
		Vessel diameter	Sex	Age at death	MRI to death interval
Venous collagenosis	**p = 0.017, β = 0.167**	p = 0.007, β = −.0181	p = 0.006, β = 0.171	p < 0.001, β = 0.509	p < 0.001, β = −0.669
Arterial collagenosis	**p = 0.128, β = 0.105**	p = 0.191, β = −0.091	p = 0.002, β = 0.192	p < 0.001, β = 0.324	p = 0.007, β = −0.173
Venous PVS width	p = 0.133, β = 0.088		p = 0.013, β = 0.159	p < 0.001, β = 0.531	p < 0.001, β = −0.705
Arterial PVS width	p = 0.937, β = 0.005		p = 0.001, β = 0.198	p < 0.001, β = 0.335	p = 0.003, β = −0.188

pulse pressure and pressure variability results in increased downstream tensile shear stress on the venous system, which is less able to manage higher pulse pressures due to the absence of a smooth muscle cell layer. In response to this shear stress, collagen is produced and deposited to strengthen and shore up the walls of veins and arteries, resulting in stiffer vessel walls which decrease the pulsatile potential of that vessel. Since fluid flow in the PVS is largely driven by pulsatile movement, bulk fluid stasis in the PVS may occur, and the concomitant decrease in fluid egress may cause interstitial fluid accumulation instantiated as pvWMH.

Like others, we found an association between female sex and greater WMH burden[25,26]), a relationship which has been thought be driven, in part, by increased arterial stiffness in women compared with men.[27,28] Interestingly, in this cohort we did not find a sex difference in venous collagenosis, a potential down-stream consequence of arterial stiffness that might explain variation in WMH burden. It is possible that differences in arterial stiffness between men and women were minimal in this population, or that other factors, including microstructural integrity differences related to sex hormone exposure[29] explain sex differences in WMH burden observed here.

It is important to note that that PVS size may not be a specific indicator of PVS clearance efficiency *or* inefficiency. In our regression models, venous collagenosis was a significant predictor of pvWMH burden and, although PVS size is correlated with collagenosis in both veins and arteries, PVS size did not predict pvWMH volumes. These results are consistent with a mechanism by which collagenosis renders veins more rigid thereby impairing perivascular and subsequently interstitial fluid flow. Enlargement of the PVS may be one result of collagenosis, as collagen fibers are situated basolaterally in the tunica externa of vessels of either lineage. However, PVS size is not necessarily an indication of flow efficiency in that same space, as the PVS may dilate for reasons unrelated to fluid flow or collagen, including inflammatory factors.[30]

Larger vessels require proportionally larger scaffolding to maintain structure and protect against pulsatile stress; vessel diameter was correlated with collagen burden in both veins and arteries. Interestingly, we did not observe a similar relationship between vessel diameter and PVS width. If the width of the PVS were a marker of the capacity to clear ISF, one might expect larger vessels to have proportionally larger PVS as the need to deliver and drain blood from a region likely correlates with the requirement to drain toxic solutes and other metabolic byproducts. However, this does not appear to be the case, again suggesting that PVS size may be a consequence or cause of a disease state such as collagenosis rather than a regular feature related to vessel size.

A final explanation for this negative finding is that PVS are related to pvWMH but that only the very largest are pathologically relevant. *In vivo* MRI imaging studies of PVS only capture the extreme upper end of PVS dilation due to the resolution limitations of MRI (at best $0.5mm^3$ but more often $1mm^3$) and often use counts of MR-visible PVS rather than continuous volume or width measurements. In contrast, this study examined the PVS width of all vessels as a continuous variable. Perhaps the inclusion of many non-pathological PVS obscured the relationship between WMH and the largest, pathologically relevant PVS, although this relationship has been most often reported as it relates to deep WMH, and not pvWMH. It is not yet known whether there exists a size threshold beyond which a PVS may be considered pathological or damaged; future studies may provide a normative distribution, which is likely to vary by location and

vessel lineage, and which would help in assigning a given PVS to a normal or abnormal classification.

In addition to the limitations already discussed, interpretation of these results should be made with caution due to methodological constraints. Vessels that were fully occluded by collagen so that no lumen hole could be identified were excluded from analysis. Vessels with an extremely thin ring of collagen that at any point thinned below our image resolution were also excluded for having broken walls; thus, both the upper and lower extremes of collagenized vessels were excluded from analysis. Due to the difficulty of clearly resolving the lumen using automated methods at scale, vessels smaller than 130 μm in diameter were not examined. This size constraint excludes smaller arterioles and future studies conducted at smaller scale may help elucidate mechanistic relationships not observed here. WMH volumes were derived from *in vivo* imaging acquired years before death (mean 6.9 years). A shorter interval between MRI and death would have yielded more accurate WMH volume measurements.

The generalizability of these finding is limited by the samples being drawn primarily from Alzheimer's disease afflicted tissue and collecting data from other cohorts would be beneficial. The mechanisms by which WMH develop and progress are likely multifactorial, particularly in an AD population in which tau and amyloid deposition may contribute.[6,31] Future studies could extend this work by coregistering and analyzing amyloid and tau staining in conjunction with vessel collagenosis. There is also anatomical heterogeneity in the presentation of vessels and WMH throughout the brain which is difficult to fully characterize at the microscopic scale; future studies acquiring samples from regions of the brain that are not periventricular, as well as samples specifically targeting MR-visible WMH are needed in order to fully capture the full breadth of factors relating to regional WMH accumulation. Additional data collected *in vivo* would also be beneficial for future studies including cardiovascular risk factors, pulse wave velocity and pulse pressure. Finally, as with any *post mortem* investigation, assertions of the specifics of dynamic processes should be avoided. While this study does not directly examine mechanistic hypotheses, it does preferentially support some putative mechanisms for the significant relationship between pvWMH and venous collagenosis, and does not support arterial collagenosis as a contributor to pvWMH burden.

Acknowledgments

Author Contributions

D.L., E.B., S.B., D.L.S., R.W., J.K., F.G., J.R., L.C.S. contributed to the conception and design of the study. D.L., D.L.S., R.W., N.R., H.D., E.B., L.C.S. contributed to the acquisition and analysis of data. D.L., D.L.S., R.W., L.C.S. contributed to the drafting of text or preparing the figures.

Potential Conflicts of Interest

Nothing to report.

References

1. Wardlaw JM, Valdes Hernandez MC, Munoz-Maniega S. What are white matter hyperintensities made of? Relevance to vascular cognitive impairment. J Am Heart Assoc 2015;4:001140.

2. Silbert LC, Howieson DB, Dodge H, Kaye JA. Cognitive impairment risk: white matter hyperintensity progression matters. Neurology 2009;73:120–125.

3. DeCarli C, Murphy DGM, Tranh M, et al. The effect of white matter hyperintensity volume on brain structure, cognitive performance, and cerebral metabolism of glucose in 51 healthy adults. Neurology 1995;45:2077–2084.

4. Debette S, Markus HS. The clinical importance of white matter hyperintensities on brain magnetic resonance imaging: systematic review and meta-analysis. BMJ 2010;341:c3666.

5. Fazekas F, Schmidt R, Scheltens P. Pathophysiologic mechanisms in the development of age-related white matter changes of the brain. Dement Geriatr Cogn Disord 1998;9:2–5.

6. Erten-Lyons D, Woltjer R, Kaye J, et al. Neuropathologic basis of white matter hyperintensity accumulation with advanced age. Neurology 2013;81:977–983.

7. Black S, Gao F, Bilbao J. Understanding white matter disease: imaging-pathological correlations in vascular cognitive impairment. Stroke 2009;40:S48–S52.

8. Fernando MS, Simpson JE, Matthews F, et al. White matter lesions in an unselected cohort of the elderly: molecular pathology suggests origin from chronic hypoperfusion injury. Stroke 2006;37:1391–1398.

9. Gouw AA, Seewann A, van der Flier WM, et al. Heterogeneity of small vessel disease: a systematic review of MRI and histopathology correlations. J Neurol Neurosurg Psychiatry 2011;82:126–135.

10. Young VG, Halliday GM, Kril JJ. Neuropathologic correlates of white matter hyperintensities. Neurology 2008;71:804–811.

11. Moody DM, Brown WR, Challa VR, Anderson RL. Periventricular venous collagenosis: association with leukoaraiosis. Radiology 1995; 194:469–476.

12. Nan D et al. Potential mechanism of venous system for Leukoaraiosis: from post-mortem to in vivo research. Neurodegener Dis 2019;19:101–108.

13. Zhou M, Mao L, Wang Y, et al. Morphologic changes of cerebral veins in hypertensive rats: venous collagenosis is associated with hypertension. J Stroke Cerebrovasc Dis 2015;24:530–536.

14. Lin J, Lan L, Wang D, et al. Cerebral venous collagen remodeling in a modified White matter lesions animal model. Neuroscience 2017; 367:72–84.

15. Keith J, Gao FQ, Noor R, et al. Collagenosis of the deep medullary veins: an Underrecognized pathologic correlate of White matter Hyperintensities and periventricular infarction? J Neuropathol Exp Neurol 2017;76:299–312.

16. Rennels ML, Gregory TF, Blaumanis OR, et al. Evidence for a 'paravascular' fluid circulation in the mammalian central nervous system, provided by the rapid distribution of tracer protein throughout the brain from the subarachnoid space. Brain Res 1985;326:47–63.

17. Iliff JJ, Wang M, Liao Y, et al. A paravascular pathway facilitates CSF flow through the brain parenchyma and the clearance of interstitial solutes, including amyloid beta. Sci Transl Med 2012;4:147ra111.

18. Silbert LC, Nelson C, Howieson DB, et al. Impact of white matter hyperintensity volume progression on rate of cognitive and motor decline. Neurology 2008;71:108–113.

19. Vonsattel JP et al. Cerebral amyloid angiopathy without and with cerebral hemorrhages: a comparative histological study. Ann Neurol 1991;30:637–649.

20. White L et al. Cerebrovascular pathology and dementia in autopsied Honolulu-Asia aging study participants. Ann N Y Acad Sci 2002;977: 9–23.

21. Mueller EA, Moore MM, Kerr DCR, et al. Brain volume preserved in healthy elderly through the eleventh decade. Neurology 1998;51: 1555–1562.

22. Kaplan HA. The transcerebral venous system. An anatomical study. Arch Neurol 1959;1:148–152.

23. Pettersen JA, Keith J, Gao F, et al. CADASIL accelerated by acute hypotension: arterial and venous contribution to leukoaraiosis. Neurology 2017;88:1077–1080.

24. Todd KL et al. Ventricular and periventricular anomalies in the aging and cognitively impaired brain. Front Aging Neurosci 2017;9:445.

25. Fatemi F, Kantarci K, Graff-Radford J, et al. Sex differences in cerebrovascular pathologies on FLAIR in cognitively unimpaired elderly. Neurology 2018;90:e466–e473.

26. Sachdev PS, Parslow R, Wen W, et al. Sex differences in the causes and consequences of white matter hyperintensities. Neurobiol Aging 2009;30:946–956.

27. Berry KL, Cameron JD, Dart AM, et al. Large-artery stiffness contributes to the greater prevalence of systolic hypertension in elderly women. J Am Geriatr Soc 2004;52:368–373.

28. Coutinho T. Arterial stiffness and its clinical implications in women. Can J Cardiol 2014;30:756–764.

29. van Hemmen J, Saris IMJ, Cohen-Kettenis PT, et al. Sex differences in White matter microstructure in the human brain predominantly reflect differences in sex hormone exposure. Cereb Cortex 2017;27: 2994–3001.

30. Wuerfel J, Haertle M, Waiczies H, et al. Perivascular spaces--MRI marker of inflammatory activity in the brain? Brain 2008;131:2332–2340.

31. Lee S, Viqar F, Zimmerman ME, et al. White matter hyperintensities are a core feature of Alzheimer's disease: evidence from the dominantly inherited Alzheimer network. Ann Neurol 2016;79:929–939.